Structural insights into the antigenicity of myelin oligodendrocyte glycoprotein

Constanze Breithaupt*†, Anna Schubart‡§, Hilke Zander¶, Arne Skerra¶, Robert Huber*, Christopher Linington‡‖, and Uwe Jacob*

*Abteilung Strukturforschung, Max-Planck-Institut für Biochemie, Am Klopferspitz 18a, 82152 Martinsried, Germany; ‡Abteilung Neuroimmunologie, Max-Planck-Institut für Neurobiologie, Am Klopferspitz 18a, 82152 Martinsried, Germany; and ¶Lehrstuhl für Biologische Chemie, Technische Universität München, 85350 Freising-Weihenstephan, Germany

Contributed by Robert Huber, June 6, 2003

Multiple sclerosis is a chronic disease of the central nervous system (CNS) characterized by inflammation, demyelination, and axonal loss. The immunopathogenesis of demyelination in multiple sclerosis involves an autoantibody response to myelin oligodendrocyte glycoprotein (MOG), a type I transmembrane protein located at the surface of CNS myelin. Here we present the crystal structures of the extracellular domain of MOG (MOG^{Igd}) at 1.45-Å resolution and the complex of MOG^{Igd} with the antigen-binding fragment (Fab) of the MOG-specific demyelinating monoclonal antibody 8-18C5 at 3.0-Å resolution. MOG^{Igd} adopts an IgV like fold with the A′GFCC′C″ sheet harboring a cavity similar to the one used by the costimulatory molecule B7-2 to bind its ligand CTLA4. The antibody 8-18C5 binds to three loops located at the membrane-distal side of MOG with a surprisingly dominant contribution made by MOG residues 101–108 containing a strained loop that forms the upper edge of the putative ligand binding site. The sequence R^{101}DHSYQEE^{108} is unique for MOG, whereas large parts of the remaining sequence are conserved in potentially tolerogenic MOG homologues expressed outside the immuno-privileged environment of the CNS. Strikingly, the only sequence identical to DHSYQEE was found in a *Chlamydia trachomatis* protein of unknown function, raising the possibility that *Chlamydia* infections may play a role in the MOG-specific autoimmune response in man. Our data provide the structural basis for the development of diagnostic and therapeutic strategies targeting the pathogenic autoantibody response to MOG.

Multiple sclerosis (MS) is a chronic inflammatory and demyelinating disease of the central nervous system (CNS) associated with autoaggressive T and B cell responses to various myelin proteins. Myelin oligodendrocyte glycoprotein (MOG) was identified as a candidate autoantigen in MS because it induces a demyelinating antibody response in laboratory animals with experimental autoimmune encephalomyelitis (EAE), an animal model of MS (1). MOG is a quantitatively minor type I transmembrane CNS protein of unknown function with a single extracellular Ig-like domain (2). In contrast to other CNS proteins, MOG is found only in mammals and is highly conserved across species. It is expressed exclusively in the CNS by myelin-forming oligodendrocytes and is preferentially localized at the outermost surface of the myelin sheath thus directly exposed to autoantibodies in the extracellular milieu. MOG is the only antigen that can induce both a pathogenic demyelinating autoantibody response and an encephalitogenic T cell response in experimental animals (3). In MOG-induced EAE this combination of immune effector mechanisms reproduces the demyelinating pathology seen in the majority of patients with MS. The clinical relevance of autoimmune responses to MOG in MS is supported by reports that MS is associated with enhanced MOG-specific T and B cell responses and by the identification of MOG-specific antibodies associated with myelin debris in actively demyelinating MS lesions (4). Experimental evidence indicates that the autoantibody response to MOG is heterogeneous; demyelinating MOG-specific autoantibodies recognize purely conformation-dependent epitopes whereas MOG peptide-specific antibodies fail to recognize the native protein (5–7). To examine the structural basis of the pathogenic autoantibody response to MOG we determined the crystal structures of the extracellular domain of rat MOG (residues 1–126, MOG^{Igd}) and a complex of MOG^{Igd} with the chimeric antigen-binding fragment (Fab) of the demyelinating MOG-specific monoclonal antibody 8-18C5 (8).

Materials and Methods

Preparation of Recombinant MOG^{Igd} and the MOG^{Igd}–(8-18C5)-Fab Complex. The cDNA of the extracellular domain of rat MOG (residues 1–125) was subcloned into the His-tag expression vector pQE-12. The protein was overexpressed in inclusion bodies in *Escherichia coli*, refolded, and further purified by nickel-nitrilotriacetic acid affinity chromatography and gel filtration. Selenomethionine (SeMet)-labeled protein was produced in the methionine-auxotrophic *E. coli* strain B834(DE3) and grown in minimal medium with SeMet (0.3 mM) substituted for methionine. The cDNA of the variable domains of the mouse monoclonal antibody 8-18C5 was subcloned into the expression vector pASK107, yielding the chimeric (8-18C5)-Fab composed of the 8-18C5 variable domains, the human IgG constant domains, and the Strep tag II fused to the C terminus of the heavy chain (9, 10). (8-18C5)-Fab was produced by periplasmic secretion in *E. coli* and purified by streptavidin affinity chromatography and gel filtration (11). A 1:1 molar ratio of MOG^{Igd} and (8-18C5)-Fab was mixed to form the MOG^{Igd}–(8-18C5)-Fab complex followed by a final gel-filtration chromatography step.

Crystallization and Data Collection. Crystals were grown at 18°C with the sitting drop vapor diffusion method by mixing 2 μl of 5 mg/ml MOG^{Igd} or SeMet-MOG^{Igd} solution (10 mM Tris·HCl, pH 7.4/30 mM NaCl) with 1 μl of reservoir solution (100 mM Tris·HCl, pH 7.2/100 mM $MgAc_2$/22% polyethylene glycol 8000) and equilibrating against reservoir solution. The complex was crystallized by combining 2 μl of 3.5 mg/ml MOG^{Igd}–(8-18C5)-Fab solution (5 mM Mops, pH 7.5/50 mM NaCl) with 0.5 μl of reservoir solution (100 mM Tris·HCl, pH 8.5/14% polyethylene glycol 8000). The hexagonal crystals of MOG^{Igd} and SeMet-MOG^{Igd} belong to space group $P3_221$ ($a = b = 50.3$ Å, and $c = 76.6$ Å) and contain one molecule per asymmetric unit with 29% solvent. The complex crystallized in space group $P2_1$

Abbreviations: MS, multiple sclerosis; MOG, myelin oligodendrocyte glycoprotein; MOG^{Igd}, extracellular domain of MOG; EAE, experimental autoimmune encephalomyelitis; SeMet, selenomethionine; CDR, complementarity-determining region.

Data deposition: The atomic coordinates and structure factors have been deposited in the Protein Data Bank, www.rcsb.org {PDB ID codes 1PKO (SeMetMOG^{Igd}) and 1PKQ [MOG^{Igd}–(8-18C5)-Fab]}.

†To whom correspondence should be addressed. E-mail: breitha@biochem.mpg.de.

§Present address: Center for Neurological Diseases, Department of Neurology, Brigham and Women's Hospital, Harvard Medical School, Boston, MA 02115.

‖Present address: University of Aberdeen, Department of Medicine and Therapeutics, Foresterhill, Aberdeen AB25 2ZD, United Kingdom.

Table 1. Data collection and refinement statistics

Data collection		
Data set	SeMet-MOG^{Igd}	MOG^{Igd}–(8-18C5)-Fab
Resolution limit, Å	1.45	3.0
Completeness, %	99.3 (99.6)*	86.7 (73.0)*
Unique reflections	20,292	22,490
Redundancy	3.9 (3.8)	2.3 (1.9)
R_{merge}†, %	5.1 (39.8)	9.4 (35.1)
$I/\sigma(I)$	28.1 (3.9)	5.3 (2.0)
Refinement		
R_{crys}/R_{free}‡, %	19.5/21.9	25.0/31.9
Protein atoms	1,030	8,433
Water molecules	131	85
Average B factor, Å^2	20.2	33.6
rmsd: bond lengths, Å/angles, °/bonded B values§, Å^2	0.011/1.64/2.1	0.012/1.66/2.1

*Values for highest resolution shells (1.45–1.47 and 3.0–3.1 Å).
†$R_{merge} = \Sigma_h\Sigma_i|I_i(\mathbf{h}) - \langle I(\mathbf{h})\rangle|/\Sigma_h\Sigma_i I_i(\mathbf{h})$.
‡$R_{crys} = \Sigma_h||F_o(\mathbf{h})| - |F_c(\mathbf{h})||/\Sigma_h|F_o(\mathbf{h})|$.
§rms deviations (rmsd) of temperature factors of bonded atoms.

(a = 124.5 Å, b = 40.0 Å, c = 134.2 Å, and β = 107.8°) with two molecules per asymmetric unit and 47% solvent content. Diffraction data of MOG^{Igd}, SeMet-MOG^{Igd}, and the complex (λ = 1.0500 Å) as well as multiple anomalous diffraction data of SeMet-MOG^{Igd} (λ_1 = 0.9791 Å, λ_2 = 0.9795 Å, and λ_3 = 0.9500 Å) were collected at beamline BW6 at the German Electron Synchrotron (Hamburg, Germany). Data sets were integrated, scaled, and merged by using DENZO and SCALEPACK (ref. 12 and Table 1).

Structure Determination and Analysis. One of the two selenium sites in SeMet-MOG^{Igd} was determined with RSPS (13), and parameters were refined and phases calculated with MLPHARE (14). The resulting electron density at 1.9-Å resolution, improved by density modification carried out by using DM (14), enabled building of nearly the complete model of SeMet-MOG^{Igd}. Refinement of the model in CNS (15) and manual rebuilding in O (16) was performed by using a high-resolution data set of SeMet-MOG^{Igd} (1.45-Å resolution). The final model comprises 124 residues and has R values of R = 19.5%/R_{free} = 21.9%. The structure of native MOG^{Igd} determined by molecular replacement and refined against a data set of 2.2-Å resolution showed no significant differences compared with the high-resolution structure of SeMet-MOG^{Igd} that was therefore used for subsequent structural analysis.

The MOG^{Igd}–(8-18C5)-Fab structure was solved by molecular replacement by using SeMet-MOG^{Igd} and the Ig domains of Protein Data Bank entries 1B2W (17) (constant domains), 1D6V (18) (heavy-chain variable domain), and 2IMM (19) (light-chain variable domain) as search models. The positions of the Fab constant domains of one protomer were determined by Patterson search with AMORE (20). Fixing the two constant domains during translation search yielded the position of the constant domains of the second molecule with the noncrystallographic symmetry axis parallel to the cell axis a and κ = 40°, consistent with the solution of the self-rotation function. Subsequently, the positions of all constant domains were fixed for input into the likelihood-based molecular replacement program BEAST (21), which yielded correct solutions of the variable domains and MOG^{Igd} of one protomer. The remaining domains were clearly visible in the resulting electron-density map. Refinement in CNS was performed with restrained noncrystallographic symmetry imposed on the individual Ig domains excluding N and C termini and the hinge regions of heavy and light chains. Averaged SigmaA-weighted and composite-omit ($2F_o - F_c$) maps were used for manual rebuilding in O. During refinement, R values dropped from R = 40.6%/R_{free} = 41.3% to R = 25.0%/R_{free} = 31.8%, yielding the final model that comprises 561 residues. Calculation of atomic contacts and solvent-accessible surfaces was performed with the CCP4 package (14), searches for related sequences were done with BLAST (www.ncbi.nlm.nih.gov), and sequence and structural alignments were performed with GCG (Wisconsin Package, version 10.3, Accelrys, San Diego) and LSQMAN (22), respectively. Figures were prepared with MOLSCRIPT (23), RASTER3D (24), GRASP (25), and ALSCRIPT (26).

Results and Discussion

Overall Structure of MOG^{Igd}. MOG^{Igd} adopts a classical IgV-like fold consisting of a sandwich of two antiparallel β-sheets that comprise strands A′GFCC′C″ and ABED, respectively (Fig. 1 *a* and *b*). The glycosylation site of MOG, Asn-31, is located in the loop connecting the B and C strands (BC loop), exposed at the top, membrane-distal side of MOG^{Igd}. MOG^{Igd} is monomeric in the crystal and exhibits a predominantly polar surface that lacks any large hydrophobic or positively charged patches, suggesting that MOG^{Igd} does not interact directly with the phospholipid membrane. The main protein–protein contacts formed by MOG^{Igd} in the densely packed crystal are nonphysiological interactions of the C-terminal tail (residues 116–126) with crystallographic neighbors. Because of those stabilizing interactions the C terminus is visible in the electron density with the last ordered residue, Val-126, corresponding to the first residue of the predicted membrane-spanning helix. MOG is structurally similar to other IgV domains such as the peripheral nerve system protein P_{zero} (27), the IgV domains of the $\gamma\delta$-T cell receptor (28), and various variable antibody domains. The nearest structural neighbors of MOG are the N-terminal domains of the costimulatory molecule B7-2 (29) (CD86) and sialoadhesin (30), which superimpose with MOG with rms deviations of 1.18 and 1.37 Å for 97 and 100 aligned C^α atoms, respectively.

Functional Implications. Despite its important role as target antigen in EAE and MS, the physiological function of MOG is unknown. It has been suggested that MOG acts as an adhesion or signaling molecule or as an activator of the complement cascade by binding the complement component C1q (2). Intriguingly, B7-2 and MOG both exhibit a very short C″ strand and share the twisted conformation of the C″D loop, which constitutes one edge of a shallow cavity built by the A′GFCC′C″ sheet (Fig. 1*c*). In B7-2 this cavity is utilized to bind CTLA4 (29). The IgV domains of B7-2 and MOG that are both encoded within the MHC show sequence identities of 27%, but the amino acids that contribute to the formation of the cavity are not conserved between MOG and B7-2. Despite this lack of conservation, the cavities of both molecules exhibit a similar hydrophobic center enclosed by polar residues, suggesting that this region of MOG^{Igd} may act as a binding site for an as-yet-unidentified ligand. The C1q-binding site of mouse IgG2 has been mapped to the sequence EXKXK, located in the F strand of the second constant Ig domain of the IgG2 heavy chain (31). A similar sequence can be identified in the Ig domain of MOG (E^{64}YRGR^{68}), and it has been demonstrated that MOG binds C1q, leading to activation of complement *in vitro* (32). The structure of MOG^{Igd} reveals that the proposed C1q complement-binding site is orientated toward the membrane surface and forms two antiparallel tight turns (Fig. 1*c*), adopting a conformation that differs completely from the extended conformation of the original C1q-activating sequence in IgG2, indicating that complement activation is not the normal physiological function of MOG.

Antigenicity of MOG^{Igd}. The three-dimensional structure of MOG^{Igd} allows us to identify solvent-exposed surfaces that may

IMMUNOLOGY

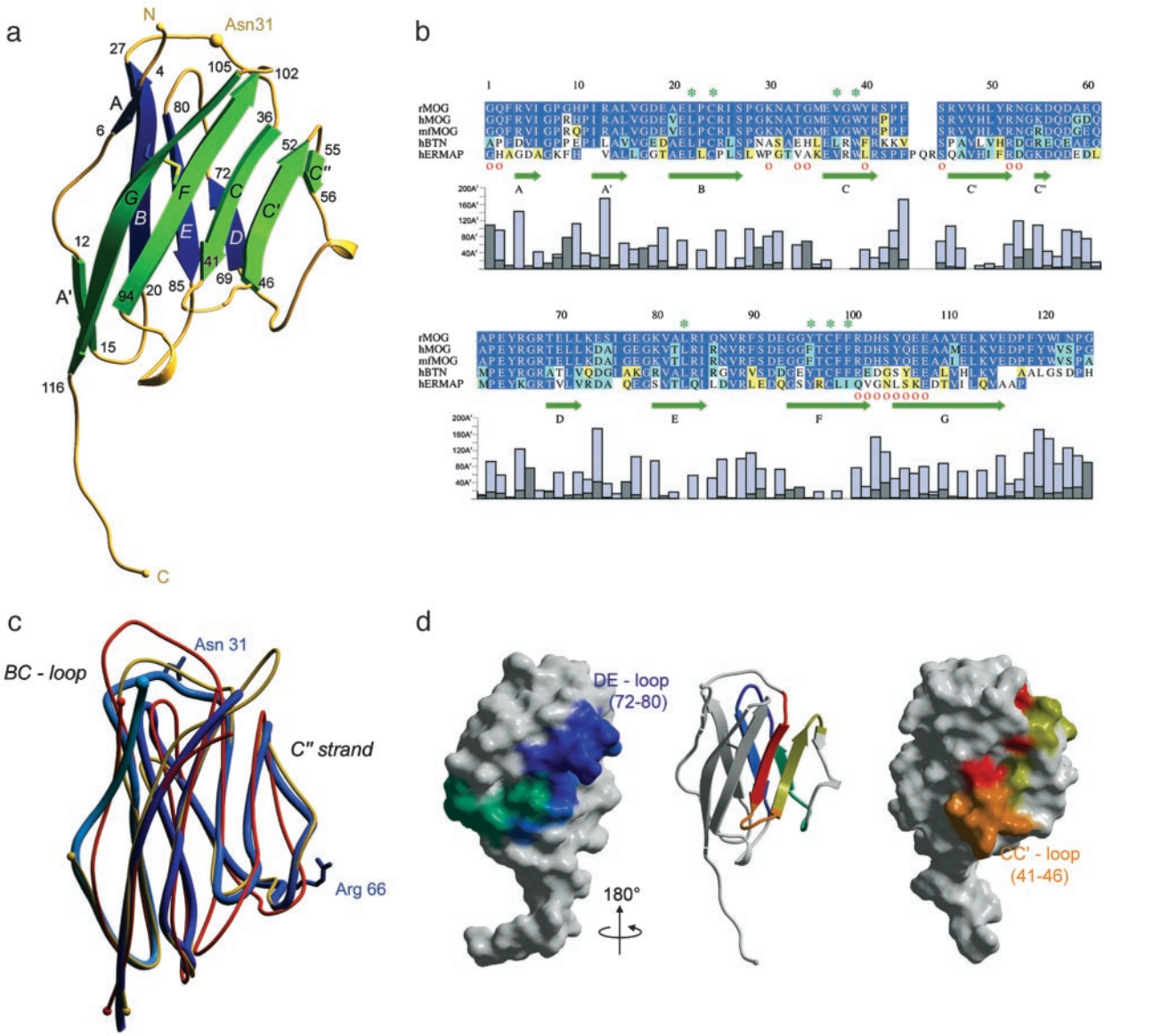

Fig. 1. Structure of the extracellular domain of MOG. (*a*) Ribbon diagram of the overall structure. Asn-31 represents the single glycosylation site of MOG positioned at the top of the molecule. (*b*) Sequence alignment of MOG from different species (rMOG, rat; hMOG, human; mfMOG, *Macaca fascicularis*) and of the related proteins butyrophilin (BTN) and erythroid membrane-associated protein (ERMAP). Residues conserved for IgV-like proteins are labeled in green (*). Red circles indicate residues of rat MOG in contact with the monoclonal antibody 8-18C5. (*Lower*) The solvent-accessible surface area per residue of uncomplexed MOG^{Igd} is shown (gray, contribution of the main chain; light blue, contribution of the side chain). (*c*) Superposition of the IgV domains of MOG (blue), P_{zero} (red), and B7-2 (yellow). In contrast to P_{zero}, MOG^{Igd} does not exhibit an extended BC loop that is assumed to be used by P_{zero} for direct interactions with the opposing myelin membrane in the peripheral nerve system. (*d*) Representation of two suggested continuous epitopes of MOG (7, 33). Residues 73–87 are depicted in green and dark and light blue, and residues 35–55 are depicted in yellow, orange, and red.

provide targets for autoantibody-mediated demyelination (Fig. 1*b*). The specificity of anti-MOG autoantibodies with demyelinating activity is strongly biased toward conformation-dependent epitopes, but the regions of MOG that support this response are unknown. One exception is a minor subset of conformation-dependent murine monoclonal antibodies that bind MOG as well as peptides containing amino acids 63–87 (7). This sequence encompasses the DE loop (amino acids 72–80), which contains highly exposed residues and forms part of a protruding surface at the top of the BED sheet, consistent with forming a minor, partially sequential epitope (Fig. 1*d*). In addition, Lewis rats immunized with the MOG peptide (amino acids 35–55) develop a demyelinating variant of EAE that led to the assumption that this sequence contains a pathogenic B cell epitope (33). Because of the concave surface of the A′GFCC′C″ sheet, the C and C′ strands are largely buried (Fig. 1 *b* and *d*), whereas the protruding CC′ loop (amino acids 41–46) is surface-exposed and highly flexible in the crystal structure, and thus available to bind antibodies.

Structure of the MOG^{Igd}–(8-18C5)-Fab Complex. To gain further insight into the nature of the discontinuous MOG epitopes recognized by pathogenic antibodies we crystallized a complex of MOG^{Igd} with a chimeric Fab derived from the demyelinating mouse monoclonal antibody 8-18C5. The antibody 8-18C5 mediates demyelination *in vitro* and *in vivo* and augments clinical EAE in rats (34). Furthermore, 8-18C5 binds MOG from several different species and inhibits the binding of 12 of a panel of 15

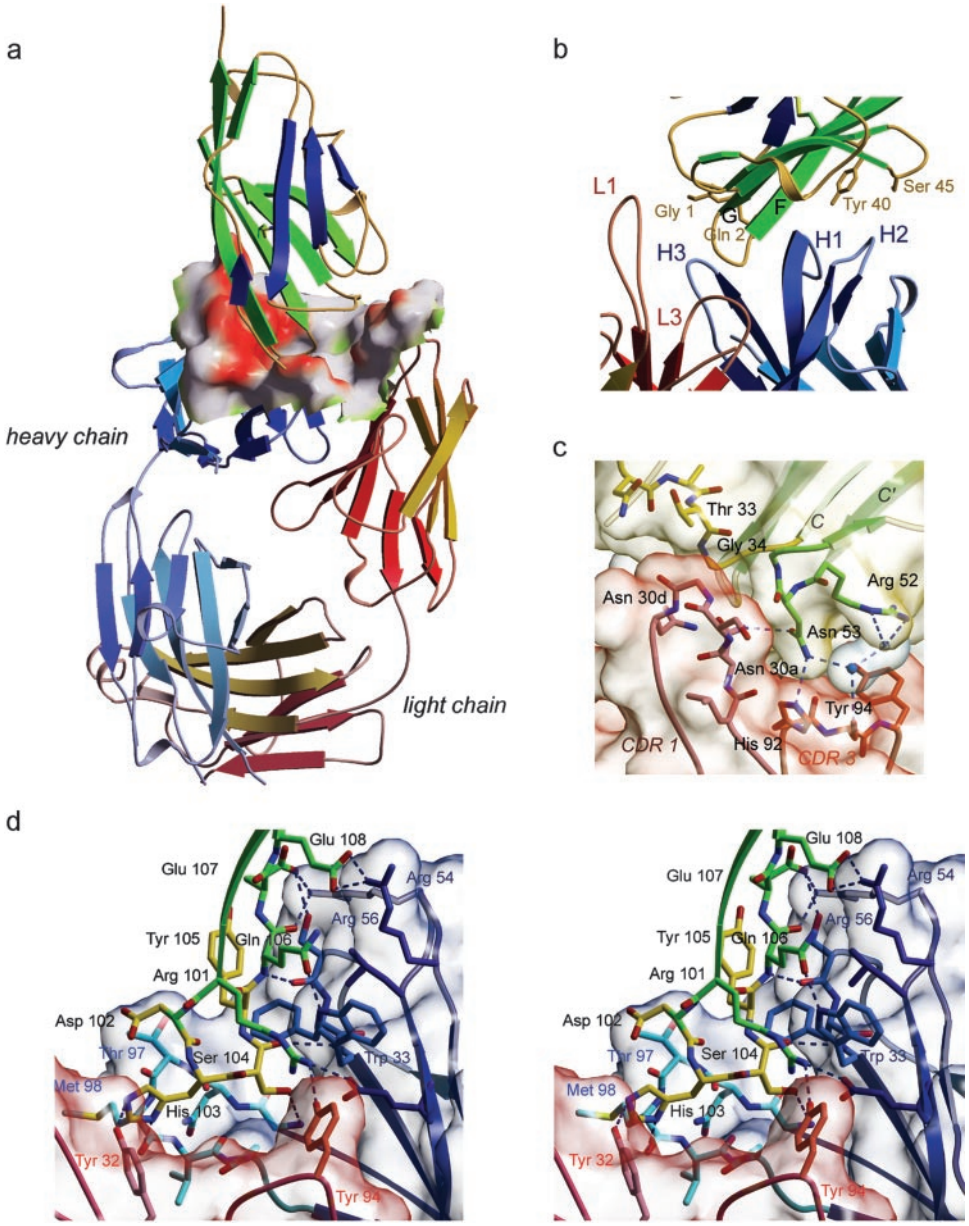

Fig. 2. Binding of the antigen-binding fragment (Fab) of 8-18C5 to MOG. (*a*) Overall structure of the Fab–MOG^{Igd} complex. The binding site of 8-18C5, shown as surface representation with atoms contacting MOG^{Igd} colored red, reveals the dominant contribution of the heavy chain to the binding of MOG. (*b*) The MOG–(8-18C5) interface. Residues Gly-1, Gln-2, Tyr-40, and Ser-45, which form the edges of the epitope, are shown as stick models. (*c*) Detailed view of the MOG–(8-18C5) light-chain interface. (*d*) Stereo view of MOG residues 101–108 binding into the cavity built by the three heavy-chain CDRs and the light-chain tyrosines Tyr-32 and Tyr-94. FG loop residues of MOG are shown in yellow, and residues belonging to the strands F and G are shown in green.

MOG-specific mouse monoclonal antibodies to MOG (35), indicating that 8-18C5 recognizes a central conserved epitope of MOG.

The crystal structure of the MOG–Fab complex reveals that 8-18C5 binds to the upper, membrane-distal surface of MOG^{Igd} interacting with the BC, C′C″, and FG loops and the N terminus of MOG. The accessible surface area of MOG^{Igd} buried by antibody binding amounts to 815 Å^2, which is in the normal range for antibody–protein interactions (36), with the dominant contribution being made by the heavy chain of 8-18C5 (Fig. 2 *a* and *b*). This is consistent with the observation that in mice transgenic for the heavy chain of 8-18C5 MOG binding is maintained by pairing this heavy chain with different endogenous light chains (37).

Interactions of the light chain with MOG^{Igd} are restricted to the complementarity-determining region 1 (CDR1) and to the CDR3 residues 92–94. The former binds the BC and the C′C″ loops via interactions with the MOG residues Thr-33, Gly-34, Asn-53, and Gly-54 (Fig. 2*c*). In addition, Asn-53 forms two hydrogen bonds to Fab light-chain residues. CDR1 and CDR3 of the 8-18C5 light chain are identical to the corresponding regions of their germ-line sequence (IgVκ 8–28); a remarkable feature of CDR1, however, is its length of 17 residues, the maximum observed for Vκ-CDR1 sequences (38), which enables CDR1 to form contacts to MOG residues distant from the center of the binding site.

The major interaction site of MOG^{Igd} and 8-18C5 is formed by the three CDRs of the heavy chain and residues of the G strand of

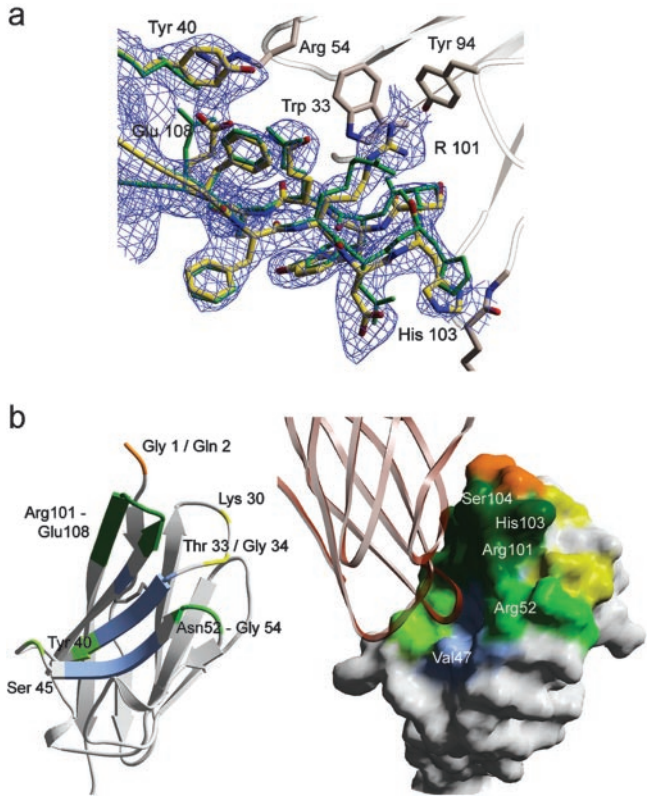

Fig. 3. The FG loop region of MOG^{Igd}. (*a*) Superposition of residues 101–108 of free (green) and complexed (yellow) MOG^{Igd}. The C$^{\alpha}$ trace of the FG loop is displaced slightly toward the heavy-chain CDRs in the MOG^{Igd}–Fab complex. In the complex the side chains of MOG residues Tyr-40, Arg-101, His-103, and Glu-108 are reoriented to optimize interactions with 8-18C5 residues. The ($2F_o - F_c$) omit electron-density map of the complex was calculated at 3.0-Å resolution by omitting MOG residues 101–108 and was contoured at 1.0 σ. (*b*) Representation of MOG^{Igd} showing the discontinuous 8-18C5 epitope at the upper surface of MOG and the putative ligand binding site. Residues that are involved in interactions with 8-18C5 are colored from orange to green according to their position in the MOG sequence, and residues forming the B7-2-like cavity are shown in light blue. The highly accessible loop residues His-103 and Ser-104 protrude from the upper surface of MOG. In addition, the C$^{\alpha}$ trace of CTLA4, positioned by superimposing the coordinates of MOG^{Igd} and the N-terminal domain of B7-2 complexed with CTLA4, is shown in light red.

MOG^{Igd} and the preceding FG loop (amino acids 101–108) that account for 65% of the total interaction surface of MOG^{Igd}. By binding to 8-18C5, the FG loop of MOG becomes completely buried in a cavity formed by the three heavy-chain CDRs (H1–H3) and Tyr-32 and Tyr-94 of the light chain (Fig. 2*d*). Asp-102, His-103, and Ser-104 occupy the bottom of this cavity and form numerous hydrophobic and polar interactions with H3. The MOG residues Ser-104 and Gln-106 are fixed by main-chain hydrogen bonds to H1 (Ser-31 and Trp-33), thus establishing a short intermolecular β-sheet. Strong hydrogen bonds are formed between the side chains of Glu-107 and Glu-108 and of the non-germ-line H2 residues Arg-54 and Arg-56, respectively, as well as between residues of the FG loop and the surrounding CDRs (Fig. 2*d*). The highly specific binding of the sequence 101–108 is further supported by van der Waals interactions of several MOG residues with the Fab heavy chain in the periphery of the binding site (Fig. 2*b*). Compared with the structure of uncomplexed MOG^{Igd}, the FG loop of MOG^{Igd} is slightly displaced after antibody binding, and several MOG^{Igd} side chains are repositioned to enable optimal binding to 8-18C5 residues (Fig. 3*a*).

MOG Interface Residues 101–108. While it was anticipated that the MOG epitope recognized by 8-18C5 would be highly discontinuous (Fig. 3*b*), the dominant role of the sequence 101–108 that comprises the FG loop is surprising. The FG loop that protrudes from the top of the Ig domain forms a hairpin loop classified as a II′ β-turn. The second position of II′ β-turns is normally a glycine (39) in MOG^{Igd}; however, it is occupied by His-103, which results in a strained loop conformation with dihedral angles of His-103 in forbidden regions of the Ramachandran plot. This provides a simple explanation for the failure to detect this antigenic region by peptide mapping with linear peptides that are unable to reproduce this strained loop structure.

Residues with strained conformations are often positioned at functionally important sites in proteins. Intriguingly, the FG loop forms the upper boundary of the B7-2-like cavity described above, supporting the idea that this cavity is involved in binding a ligand (Fig. 3*b*). This putative interaction would be perturbed when 8-18C5 binds to MOG. Interestingly, binding of 8-18C5 to MOG on the surface of oligodendrocytes leads to microtubule depolymerization *in vitro*, suggesting a role of MOG in the organization of the cytoskeleton that is compromised by binding of 8-18C5 (40).

The identification of the MOG epitope recognized by 8-18C5 provides a structural basis to investigate genetic and environmental factors that may influence the MOG-specific antibody response *in vivo*. MOG is expressed within the immunologically privileged environment of the CNS where it is sequestered from normal lymphocyte trafficking and unable to trigger antigen-specific B cell tolerance. The composition of the anti-MOG B cell repertoire, however, can be influenced by other self-antigens (37), which may include homologous proteins such as butyrophilin (41) or erythroid membrane-associated protein (42), the N-terminal IgV-like domains of which exhibit sequence identities to MOG^{Igd} of 45–55% (43). Strikingly, those residues bound by 8-18C5, an antibody that has escaped this tolerogenic influence, are least conserved between MOG and its relatives (Fig. 1*b*).

Sequence differences between MOG^{Igd} and its homologues are most pronounced within the sequence R^{101}DHSYQEE^{108}, indicating that tolerance to this region of MOG will be poorly developed. In this case, molecular mimicry involving related sequences derived from microbial pathogens may trigger a pathogenic antibody response to this region of MOG. Intriguingly, a BLAST search for sequences similar to R^{101}DHSYQEE^{108} identified several amino sequences in proteins from *Chlamydia* sp., a microorganism previously associated with MS (44, 45). The first hit of the similarity search was the sequence D^{253}HSYQEE^{259} in an uncharacterized protein, CT863, from *Chlamydia trachomatis*. This sequence is located in a region that lacks recognizable structural motifs and is predicted to be solvent-exposed and to adopt a coiled conformation raising the possibility that these residues can adopt a turn-like structure similar to that seen in MOG^{Igd}. CT863 is also present in the genome of *Chlamydia pneumonia*, the *Chlamydia* species specifically associated with MS, but genomic sequencing suggests that this particular amino acid sequence is not conserved between species. However, the BLAST search revealed a second, more-distantly related sequence, E^{379}HSYQEQ^{385}, in the *C. pneumonia* protein CT768. Based on these structural and sequence correlations, further studies are required to determine whether immunity to *C. pneumonia* can trigger a potentially pathogenic antibody response to MOG.

Overall, our data provide a structural basis for understanding the pathogenic autoantibody response to MOG. The solution of the three-dimensional structure of MOG and the identification of the FG loop as a dominant component of the epitope recognized by 8-18C5 provide a starting point for the development of diagnostic and therapeutic strategies targeting MOG in MS.

We thank Gleb Bourenkov of the Deutsche Elektronen Synchrotron (Hamburg, Germany) for assistance during data collection. This work was supported by the European Union (Biomed 2: Contract BMH4-97-2027) and Deutsche Forschungsgemeinschaft Grant SFB571 (to C.L.).

1. Bernard, C. C. A., Johns, T. G., Slavin, A., Ichikawa, M., Ewing, C., Liu, J. & Bettadapura, J. (1997) *J. Mol. Med.* **75,** 77–88.
2. Johns, T. G. & Bernard, C. C. A. (1999) *J. Neurochem.* **72,** 1–9.
3. Iglesias, A., Bauer, J., Litzenburger, T., Schubart, A. & Linington, C. (2001) *Glia* **36,** 220–234.
4. Genain, C. P., Cannella, B., Hauser, S. L. & Raine, C. S. (1999) *Nat. Med.* **5,** 170–175.
5. Haase, C. G., Guggenmos, J., Brehm, U., Andersson, M., Olsson, T., Reindl, M., Schneidewind, J. M., Zettl, U. K., Heidenreich, F., Berger, T., *et al*. (2001) *J. Neuroimmunol.* **114,** 220–225.
6. von Budingen, H. C., Hauser, S. L., Fuhrmann, A., Nabavi, C. B., Lee, J. I. & Genain, C. P. (2002) *Proc. Natl. Acad. Sci. USA* **99,** 8207–8212.
7. Brehm, U., Piddlesden, S. J., Gardinier, M. V. & Linington, C. (1999) *J. Neuroimmunol.* **97,** 9–15.
8. Linnington, C., Webb, M. & Woodhams, P. L. (1984) *J. Neuroimmunol.* **6,** 387–396.
9. Bandtlow, C., Schiweck, W., Tai, H. H., Schwab, M. E. & Skerra, A. (1996) *Eur. J. Biochem.* **241,** 468–475.
10. Fiedler, M., Horn, C., Bandtlow, C., Schwab, M. E. & Skerra, A. (2002) *Protein Eng.* **15,** 931–941.
11. Skerra, A. & Schmidt, T. G. (2000) *Methods Enzymol.* **326,** 271–304.
12. Otwinowsky, Z. & Minor, W. (1993) DENZO: A Film-Processing Program For Macromolecular Crystallography (Yale Univ. Press, New Haven, CT).
13. Knight, S. D. (2000) *Acta Crystallogr. D* **56,** 42–47.
14. Bailey, S. (1994) *Acta Crystallogr. D* **50,** 760–763.
15. Brunger, A. T., Adams, P. D., Clore, G. M., DeLano, W. L., Gros, P., Grosse-Kunstleve, R. W., Jiang, J. S., Kuszewski, J., Nilges, M., Pannu, N. S., *et al*. (1998) *Acta Crystallogr. D* **54,** 905–921.
16. Jones, T. A., Zou, J. Y., Cowan, S. W. & Kjeldgaard, M. (1991) *Acta Crystallogr. A* **47,** 110–119.
17. Fan, Z. C., Shan, L., Goldsteen, B. Z., Guddat, L. W., Thakur, A., Landolfi, N. F., Co, M. S., Vasquez, M., Queen, C., Ramsland, P. A. & Edmundson, A. B. (1999) *J. Mol. Recognit.* **12,** 19–32.
18. Mundorff, E. C., Hanson, M. A., Varvak, A., Ulrich, H., Schulz, P. G. & Stevens, R. C. (2000) *Biochemistry* **39,** 627–632.
19. Steipe, B., Pluckthun, A. & Huber, R. (1992) *J. Mol. Biol.* **225,** 739–753.
20. Navaza, J. (1994) *Acta Crystallogr. A* **50,** 157–163.
21. Read, R. J. (2001) *Acta Crystallogr. D* **57,** 1373–1382.
22. Kleywegt, G. J. (1996) *Acta Crystallogr. D* **52,** 842–857.
23. Kraulis, P. J. (1991) *J. Appl. Crystallogr.* **24,** 946–950.
24. Merritt, E. A. & Murphy, M. E. P. (1994) *Acta Crystallogr. D* **50,** 869–873.
25. Nicholls, A., Sharp, K. A. & Honig, B. (1991) *Proteins* **11,** 281–296.
26. Barton, G. J. (1993) *Protein Eng.* **6,** 37–40.
27. Shapiro, L., Doyle, J. P., Hensley, P., Colman, D. R. & Hendrickson, W. A. (1996) *Neuron* **17,** 435–449.
28. Allison, T. J., Winter, C. C., Fournie, J. J., Bonneville, M. & Garboczi, D. N. (2001) *Nature* **411,** 820–824.
29. Schwartz, J. C., Zhang, X., Fedorov, A. A., Nathenson, S. G. & Almo, S. C. (2001) *Nature* **410,** 604–608.
30. May, A. P., Robinson, R. C., Vinson, M., Crocker, P. R. & Jones, E. Y. (1998) *Mol. Cell* **1,** 719–728.
31. Duncan, A. R. & Winter, G. (1988) *Nature* **332,** 738–740.
32. Johns, T. G. & Bernard, C. C. (1997) *Mol. Immunol.* **34,** 33–38.
33. Ichikawa, M., Johns, T. G., Liu, J. L. & Bernard, C. C. A. (1996) *J. Immunol.* **157,** 919–926.
34. Schluesener, H. J., Sobel, R. A., Linington, C. & Weiner, H. L. (1987) *J. Immunol.* **139,** 4016–4021.
35. Piddlesden, S. (1991) Ph.D. thesis (Univ. of Wales, Cardiff, U.K.).
36. Sundberg, E. J. & Mariuzza, R. A. (2002) *Adv. Protein Chem.* **61,** 119–160.
37. Litzenburger, T., Bluthmann, H., Morales, P., Pham-Dinh, D., Dautigny, A., Wekerle, H. & Iglesias, A. (2000) *J. Immunol.* **165,** 5360–5366.
38. Allazikani, B., Lesk, A. M. & Chothia, C. (1997) *J. Mol. Biol.* **273,** 927–948.
39. Sibanda, B. L. & Thornton, J. M. (1985) *Nature* **316,** 170–174.
40. Dyer, C. A. & Matthieu, J. M. (1994) *J. Neurochem.* **62,** 777–787.
41. Stefferl, A., Schubart, A., Storch, M., Amini, A., Mather, I., Lassmann, H. & Linington, C. (2000) *J. Immunol.* **165,** 2859–2865.
42. Xu, H. X., Foltz, L., Sha, Y. S., Madlansacay, M. R., Cain, C., Lindemann, G., Vargas, J., Nagy, D., Harriman, B., Mahoney, W. & Schueler, P. A. (2001) *Genomics* **76,** 2–4.
43. Bourquin, C., Schubart, A., Tobollik, S., Mather, I., Ogg, S., Liblau, R. & Linington, C. (2003) *J. Immunol.* **171,** 455–461.
44. Moses, H., Jr., & Sriram, S. (2001) *BioDrugs* **15,** 199–206.
45. Swanborg, R. H., Whittum-Hudson, J. A. & Hudson, A. P. (2002) *Microbes Infect.* **4,** 1327–1333.